Indian Journal of Pure & Applied Physics
Vol. 58, February 2020, pp. 79-86

Heat and mass transfer analysis of casson fluid flow on a permeable riga-plate

P Loganathan* & K Deepa

Department of Mathematics, Anna University, Chennai 600 025, India

Received 28 November 2018; accepted 2 January 2020

Numerical analysis has been carried out for a casson fluid flow on a riga-plate with temperature dependent thermal conductivity. The physical model which governs the transport properties is solved numerically. This investigation emphasizes the consequence of variable thermal conductivity and electrically conducting magnetic field on the fluid flow. Rate of heat transfer is elevated, while the flow exposed to constructive case of variable thermal conductivity. The flow speed is enhanced for the improved values of modified Hartmann number. Correlation of the results with the similarity solutions declares the accuracy.

Keywords: Variable thermal conductivity, Casson fluid, Permeable riga-plate, EMHD

1 Introduction

Heat transfer through a fluid has the equivalent effect on thermal conductivity. For a fixed value of thermal conductivity, the temperature gradient is constant. So, the temperature configuration is consistent with respect to the conductivity. Whereas, variable thermal conductivity is described as a linear function of temperature and it exhibits fluctuations in the temperature. In most of the real time situations, materials with high conductivity require some structural constraints to spread over the heat from wall to the fluid. The purpose of using low conductivity material is to transfer minimum heat and usually displays insulation characteristics[1].

Many authors centralized their attention towards flow analysis on varying properties. Chaim[2] studied the impact of variable thermal conductivity on stagnation point flow and shooting method is adopted to obtain the solutions numerically. Heat transfer on an isothermal cylinder with the variable properties was examined by Uddin and Kumar[3]. Mahanti and Gaur[4] have discussed the temperature dependent properties on an isothermal plate with heat absorption effect. It was concluded that the temperature and flow speed are enhanced for high thermal conductivity regardless of destructive heat energy. Later, Loganathan *et al*.[5] and Iranian *et al*.[6] focused on variable property investigation on an unstratified and stratified medium.

*Corresponding author (E-mail: logu@annauniv.edu)

Hazarika and Hazarika[7] inspected the heat generation effect on an inclined permeable plate. Thakur and Hazarika[8] found the numerical solution of transport equations through shooting method for a micro polar fluid with constant heat flux. Srinivasacharya *et al*.[9] reported that the heat transfer rate is lowered by exalting the variable thermal conductivity parameter while analyzing thermophoresis particle deposition on a wavy surface with variable properties. Variations in Eyring-powell fluid flow subject to temperature dependent thermal conductivity was estimated through homotopic solution by Hayat *et al*.[10]

Externally applied magnetic field induces the high electrical conductivity. This phenomenon achieves the separation control of inadmissible flow behaviour[11,12]. A setup composed with an alternate arrangement of electrodes and magnets act as a boundary layer control system and it is named as riga-plate. The effect of wall parallel Lorentz force on riga-plate has been studied by Pantokratoras[13], Pantokratoras and Magyari[14]. Finite difference analysis on the aiding and opposing flow characteristics was perused by Magyari and Pantokratoras[15]. A significant finding of this investigation is that the aiding flow assists the flow to strengthen the flow speed.

Kumar *et al*.[16] inspected the three dimensional steady state analysis on chemically reacting fluid flow. Recently, some researchers explored the temperature dependent characteristics of incompressible fluid flow on Riga-plate. Shah *et al*. [17]

numerically modeled the stagnation point flow with variable thermal conductivity on a variably thickened riga-plate and heat transfer was depicted by Fourier's law. Afridi *et al*.[18] extended the variable thermal conductivity effect with viscosity on an impulsively started riga-plate under suction.

Non-Newtonian fluids exhibit the non linear behaviour while inspecting thermo-physical properties of the fluid flow. In general, pseudo plastic fluid shows a development in the rate of shear with respect to very low viscosity[19]. Casson fluid is classified as a non-newtonian fluid with yield pseudo plastic behaviour. The Casson fluid model displays an infinite rate of shear with low apparent viscosity and zero shear rates at infinite apparent viscosity. In industrial processing units, this fluid model used to illustrate the stress and deformation characteristics of the fluid flow concerning to yoghurt, tomato puree, food stuffs and biological materials[20]. Casson formulated the constitutive relation, while characterizing the dispersion of pigments in printing inks.

On account of rapid advances arising in this field, most of the literatures focused on this model. Periodic fluctuations of Casson fluid flow in a perforated channel was analysed by Srinivasa *et. al*[21]. Zaib *et al*.[22] studied the viscous dissipation effects on Casson fluid and concluded that the temperature is elevated for increased values of Eckert number. Casson fluid with variable thermal conductivity drew attention among the authors in the field of rheology. The constructive heat energy effects on a stratified medium with variable properties have been explored by Animasaun[23]. It was proclaimed that the temperature dependent thermal conductivity strengthen the speed, temperature and temperature gradient. Same sort of approach with suction was incorporated by Animasaun[24] and Animasaun *et al.*[25]. Subsequently, Radha *et al*.[26] manifested the influence of convective boundary condition on slip fluid flow under variable thermo physical properties.

Bearing all these ideas in mind, the present work imparted the perception of Casson fluid flow with the varying thermal conductivity past a Riga-plate saturated in a porous medium. Further, it is intended to facilitate interpretation of mechanical properties under variable thermal conductivity. Also, the detailed comparative study persuaded the reliability of solutions.

2 Mathematical Analysis

Laminar convective Casson fluid flow with temperature dependent thermal conductivity on a moving Riga-plate is presented on a semi-infinite domain. At first, the plate is deemed stationary, the fluid temperature and concentration maintain the asymptotic conditions and the velocity is zero. Sometime later, the plate accelerates with fixed speed u_0 at $t^* > 0$ in vertical direction against the gravitational force. This sudden movement leads to the change in velocity, temperature and concentration, i.e., the temperature of the plate raised to $T_w^* (> T_\infty^*)$ and the concentration increased to $C_w^* (> C_\infty^*)$. The temperature and concentration decays to free stream conditions and the speed drops to zero when the fluid particles are at the distant locations. The fluid flow along x direction vertically and the y direction is normal to the plate. The velocities u and v are described along vertical and horizontal directions respectively. The flow geometry is illustrated in Figs 1 (a and b). The stress strain relationship is configured as follows in literature[27- 29]:

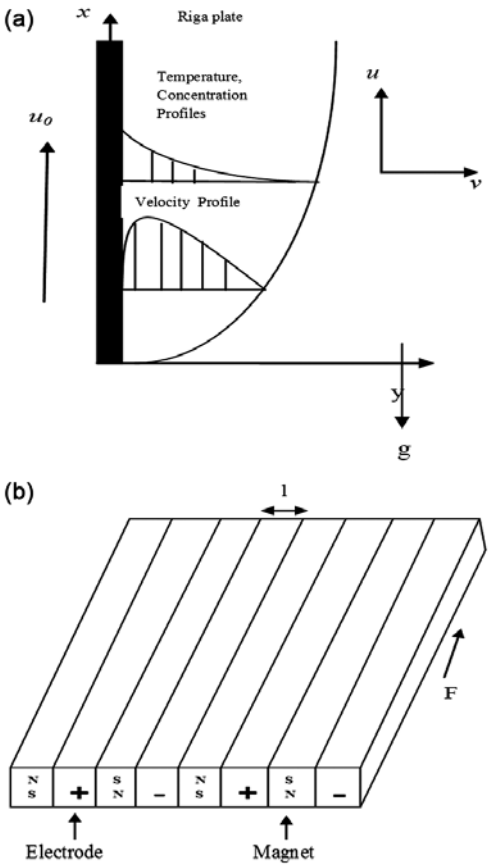

Fig. 1 – (a) Schematic representation of the flow model and (b) arrangement of electrodes and magnets.

$$\tau_{ij} = \begin{cases} 2\left(\mu_b + \frac{P_y}{\sqrt{2\pi^*}}\right) e_{ij}, \pi^* > \pi_c^* \\ 2\left(\mu_b + \frac{P_y}{\sqrt{2\pi_c^*}}\right) e_{ij}, \pi^* \leq \pi_c^* \end{cases}$$

Here, $\pi^* = e_{ij}e_{ij}$ and e_{ij} is the $(i, j)^{\text{th}}$ component of the shear rate.

The mathematical model encloses the above assumptions, constitutive equation and Boussinesq approximation can be formulated as:

$$\frac{\partial u}{\partial x} + \frac{\partial v}{\partial y} = 0 \quad \ldots (1)$$

$$\frac{\partial u}{\partial t^*} + u\frac{\partial u}{\partial x} + v\frac{\partial u}{\partial y} = \nu\left(1 + \frac{1}{\beta}\right)\frac{\partial^2 u}{\partial y^2} + g\beta'(T^* - T_\infty^*) + g\beta^*(C^* - C_\infty^*) + \frac{\pi J_0 M_0 \exp(-\pi y/l)}{8\rho} - \frac{u\nu}{\lambda^*} \cdots \quad \ldots (2)$$

$$\rho c_p\left(\frac{\partial T^*}{\partial t^*} + u\frac{\partial T^*}{\partial x} + v\frac{\partial T^*}{\partial y}\right) = \frac{\partial}{\partial y}\left(\kappa^*\frac{\partial T^*}{\partial y}\right) \quad \ldots (3)$$

$$\frac{\partial C^*}{\partial t^*} + u\frac{\partial C^*}{\partial x} + v\frac{\partial C^*}{\partial y} = D\frac{\partial^2 C^*}{\partial y^2} \quad \ldots (4)$$

Suitable initial and boundary conditions of the problem are:

$$\begin{aligned} &t^* \leq 0: u = 0, v = 0, T^* = T_\infty^*, C^* = C_\infty^* \ \forall\, x, y \geq 0 \\ &t^* > 0: u = u_0, v = 0, T^* = T_w^*, C^* = C_w^* \text{ for } y = 0 \\ &u = 0, v = 0, T^* = T_\infty^*, C^* = C_\infty^* \text{ for } x = 0 \\ &u \to 0, T^* \to T_\infty^*, C^* \to C_\infty^* \text{ as } y \to \infty \quad \cdots (5) \end{aligned}$$

Where, t^*, T^*, C^* respectively denotes the time, temperature and concentration, J_0, l and M_0 are the current density, width of the magnets and electrodes and magnetization of the magnets, u and v are vertical and horizontal velocity components, λ^* is the permeability. Here, $\beta = \frac{\mu_b\sqrt{2\pi_c^*}}{P_y}$ is the Casson parameter, μ_b, π_c^* and P_y are the plastic dynamic viscosity, critical value of π^* and yield stress respectively. In the energy balance equation, κ^*describes the thermal conductivity as linear function of temperature. According to Chaim[2], $\kappa^* = \kappa_\infty\left(1 + \epsilon^*(T^* - T_\infty^*)\right)$. While, $\epsilon = \epsilon^*(T_w^* - T_\infty^*)$, κ^* becomes $\kappa^* = \kappa_\infty(1 + \epsilon T)$. Here, ϵ denotes the variable thermal conductivity parameter and κ_∞ represents the thermal conductivity at asymptotic condition.

The transport Eqs (1, 2, 3 and 4) together with the boundary conditions (5) transformed to a non dimension form using the following quantities:

$$X = \frac{xu_0}{\nu}, Y = \frac{yu_0}{\nu}, U = \frac{u}{u_0}, V = \frac{v}{u_0}, t = \frac{t^*u_0^2}{\nu},$$
$$T = \frac{T^* - T_\infty^*}{T_w^* - T_\infty^*}, C = \frac{C^* - C_\infty^*}{C_w^* - C_\infty^*},$$
$$Gr = \frac{\nu g\beta'(T_w^* - T_\infty^*)}{u_0^3}, Gc = \frac{\nu g\beta^*(C_w^* - C_\infty^*)}{u_0^3},$$
$$Pr = \frac{\nu\rho c_p}{\kappa_\infty}, \lambda = \frac{\lambda^* u_0^2}{\nu^2}, Sc = \frac{\nu}{D}, Ha = \frac{\pi J_0 M_0 \nu}{8\rho u_0^3},$$
$$S = \frac{\pi\nu}{lu_0}$$

Dimensionless form of (1), (2), (3), (4) and (5) are given by:

$$\frac{\partial U}{\partial X} + \frac{\partial V}{\partial Y} = 0 \quad \ldots (6)$$

$$\frac{\partial U}{\partial t} + U\frac{\partial U}{\partial X} + V\frac{\partial U}{\partial Y} = \left(1 + \frac{1}{\beta}\right)\frac{\partial^2 U}{\partial Y^2} + Gr\,T + Gc\,C + Ha\,e^{-SY} - \frac{U}{\lambda} \quad \ldots (7)$$

$$\frac{\partial T}{\partial t} + U\frac{\partial T}{\partial X} + V\frac{\partial T}{\partial Y} = \frac{1}{Pr}\left((1 + \epsilon T)\frac{\partial^2 T}{\partial Y^2} + \epsilon\left(\frac{\partial T}{\partial Y}\right)^2\right) \quad \ldots (8)$$

$$\frac{\partial C}{\partial t} + U\frac{\partial C}{\partial X} + V\frac{\partial C}{\partial Y} = \frac{1}{Sc}\frac{\partial^2 C}{\partial Y^2} \cdots \quad \ldots (9)$$

Appropriate initial and boundary conditions are:

$$\begin{aligned} &t \leq 0: U = 0, V = 0, T = 0, C = 0 \ \forall\, X, Y \\ &t > 0: U = 1, V = 0, T = 1, C = 1 \text{ for } Y = 0 \\ &U = 0, V = 0, T = 0, C = 0 \text{ for } X = 0 \\ &U \to 0, T \to 0, C \to 0 \text{ as } Y \to \infty \quad \ldots (10) \end{aligned}$$

Where t, T, C, U and V describes the dimensionless time, temperature, concentration, vertical and horizontal velocity components, Pr, Gr and Gc are the Prandtl number, thermal and mass Grashof number, Ha denotes the modified Hartmann number, λ is the permeability parameter.

3 Numerical Solution

The system (6)-(10) has been solved by adopting finite difference procedure. Specifically, Crank-Nicholson implicit scheme is employed. By discretizing the coupled non linear system with the finite difference approximation of suitable order, the

set of linear algebraic equations are obtained. Thomas algorithm is executed to acquire the velocity, temperature and concentration from the algebraic equations (Carnahan *et al*.[30]).

Mesh generation and grid independence test determines the accuracy of the results. The computational domain is divided into smaller rectangles with $X_{max} = 1.0$ and $Y_{max} = 14.0$. Y_{max} represents the value of Y at the asymptotic conditions and the observed effects of the boundary layer are not significant at this point. The computational procedure continues up to the solution seizes the stead state. The variation of 0.00001 between dependent variables assures the steady state solution so that the relative error in comparison with current iteration and previous iteration is less than or equal to 0.00001. On the execution of grid independence test, the space between each grid has been continuously tested with the modifications in the sizes to check the ultimate results are independent of the grid spacing. Moreover, uniform grid spacing was carried out throughout the evaluation.

The point wise approximations are reckoned for grid spacing $\Delta X = 0.02$ and $\Delta Y = 0.2$ with $\Delta t = 0.01$ time steps. This discretization process has to validate the issues such as scheme consistency, stability of the method and convergence of the solution (Smith [31]). As the finite difference approximations of the derivatives are obtained by truncation of Taylor series to the appropriate order, the truncation error exist (D'acunto[32]). The truncation error $O(\Delta t^2 + \Delta Y^2 + \Delta X) \to 0$, when $\Delta t, \Delta Y$ and $\Delta X \to 0$. This upholds the consistency of the scheme. Stability is one of the major advantages of implicit finite difference method, because the explicit scheme is a conditionally stable scheme. Also, the explicit methods necessitate the smaller time step Δt. Even though the implicit scheme is unconditionally stable, some source terms affect the stability. The source terms incorporated in the present problem does not disrupt the stability which is ratified by Von Neumann stability analysis, i.e, the error does not increase as time increases. Thus, the method is unconditionally stable. The convergence of solutions followed from Lax-equivalence theorem, since the scheme is stable and consistent. Despite the method demands more computational effort and memory allocation, it is efficient in terms of accuracy. In actual fact, other discretization techniques apart from finite difference method entail to mesh refinement. Sometimes, an approximation over the complex geometry is difficult while employing finite difference approximation. However, the geometry which is under consideration is regular. Thus, the finite difference method is the most effective technique for this modelling.

Further, the skin friction, rate of heat and mass transfer can be calculated using numerical integration with the following relations:

$$\tau_X = -\left(1+\frac{1}{\beta}\right)\left(\frac{\partial U}{\partial Y}\right)_{Y=0}, \bar{\tau} = -\int_0^1 \left(1+\frac{1}{\beta}\right)\left(\frac{\partial U}{\partial Y}\right)_{Y=0} dX, \quad \ldots (11)$$

$$Nu_X = -X\left(\frac{\partial T}{\partial Y}\right)_{Y=0}, \overline{Nu} = -\int_0^1 \left(\frac{\partial T}{\partial Y}\right)_{Y=0} dX, \quad \ldots (12)$$

$$Sh_X = -X\left(\frac{\partial C}{\partial Y}\right)_{Y=0}, \overline{Sh} = -\int_0^1 \left(\frac{\partial C}{\partial Y}\right)_{Y=0} dX, \quad \ldots (13)$$

4 Results and Discussion

Comparison study with Gebhart and Pera[33] is carried out and elucidated in Fig. 2. This analysis is one of the earliest investigations which extensively studied the combined thermal and mass diffusion on vertical surfaces through similarity solutions. The comparison accomplishes the accuracy and reliability of the numerically evaluated solutions.

Figure 3 illustrates the velocity distribution for the pertinent parameters such as λ, ϵ and Ha. Heat transfer mechanism is greatly influenced by the thermal conductivity along transverse direction. $\kappa^*(T)$

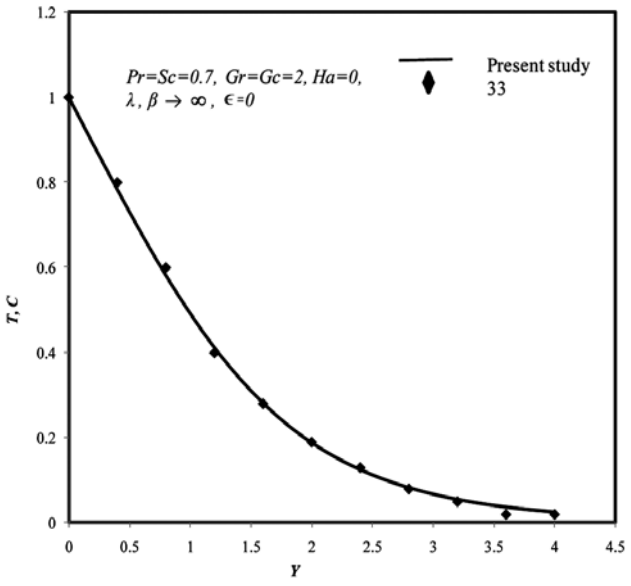

Fig. 2 – Comparison of temperature and concentration.

describes the temperature dependent thermal conductivity as a linear function. Elevation in the variable thermal conductivity parameter leads to the depletion of viscosity. Hence, the momentum boundary layer thickens considerably and the reverse characteristic is observed when $\epsilon < 0$. Owing to permeability parameter (λ), the stronger permeability dispenses the fluid with a high flow speed. The velocity field has also been reinforced by aiding flow along the direction of Lorentz force. Thus, the higher values of modified Hartmann number substantially enhance the flow velocity.

The temperature profiles are presented in Fig. 4. In the thin thermal boundary layer the transition of heat from hot surface to the colder surroundings is encountered. Thickness of this layer decides the temperature distribution throughout the fluid flow. Casson parameter β depends on the plastic dynamic viscosity and yield stress of the fluid flow. The increased fluid viscosity because of the heightened values of β diminishes the temperature. Diminution in modified Hartmann number elevates the thermal diffusion by virtue of stronger magnetic field. In general, heat energy has been greatly improved by the high physical strength of thermal conductivity. Increasing the constructive variable thermal conductivity parameter ($\epsilon > 0$) thickens the thermal boundary layer, whereas temperature declines for destructive variable thermal conductivity parameter ($\epsilon < 0$) and permeability parameter.

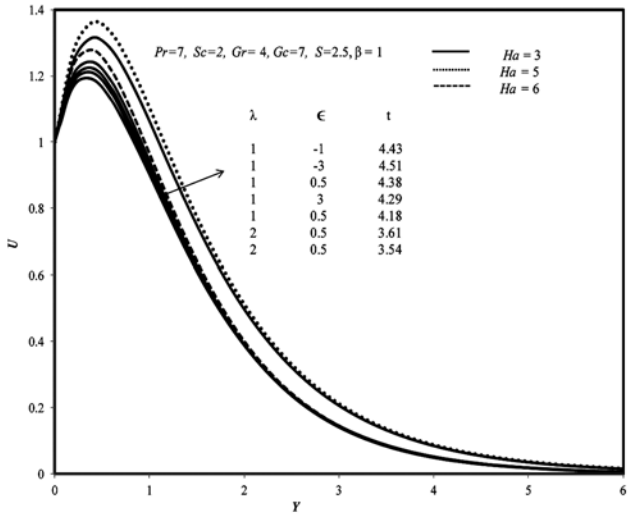

Fig. 3 – Velocity distribution for various values of λ, ϵ and *Ha*.

Variations in the concentration profiles are explored in Fig. 5. The higher mass diffusivity is observed due to the increment in Schmidt number. Displacement thickness of the mass transfer boundary layer is enlarged while exalting magnetic field strength with the heightened values of *Ha.* Concentration of the species diminished for high thermal conductivity which results in elevated variable thermal conductivity parameter.

In Figs 6 and 7, viscous drag is interpreted in local and average sense. Uplifting the values of ϵ increases the thermal conductivity which reduces the shear stress between the fluid layers. Further, hike in the values of Casson parameter induces the high skin friction. The improved values of λ expand the size of the pores so that the fluid can easily pass through the pores and approaches the plate surface with the

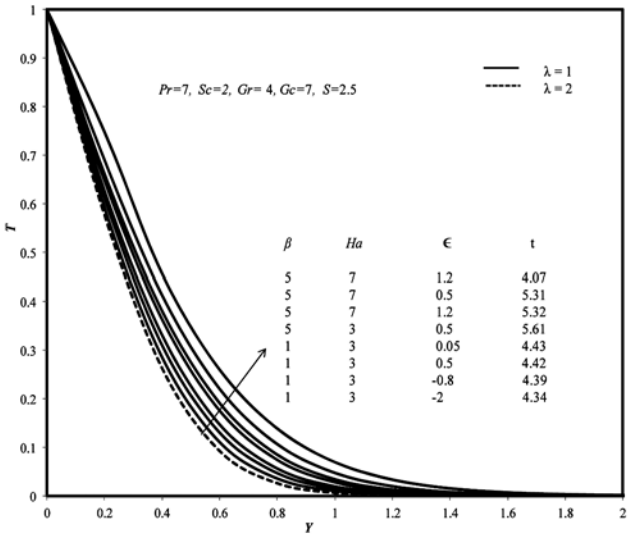

Fig. 4 – Impact of variable thermal conductivity and *Ha* on temperature field.

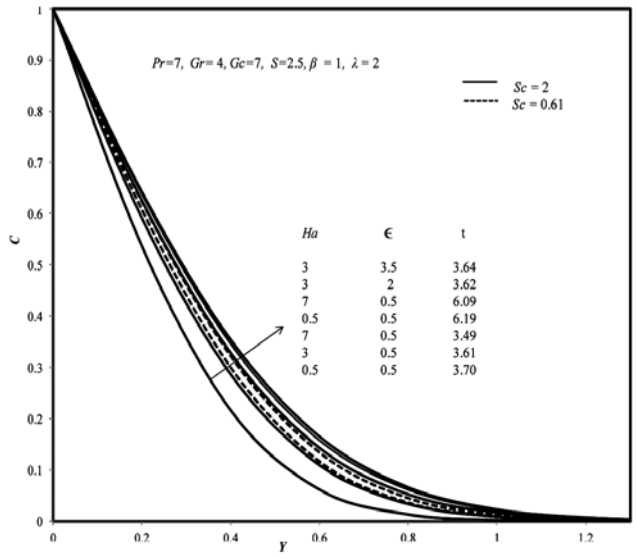

Fig. 5 – Influence of *Ha* and ϵ on mass diffusion.

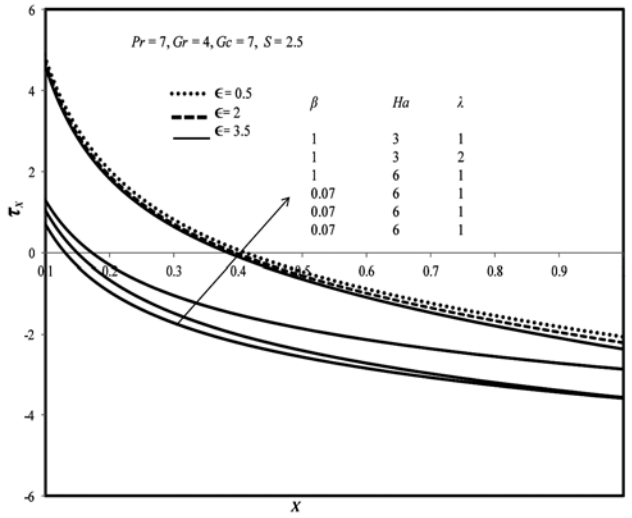

Fig. 6 – Local skin friction coefficient.

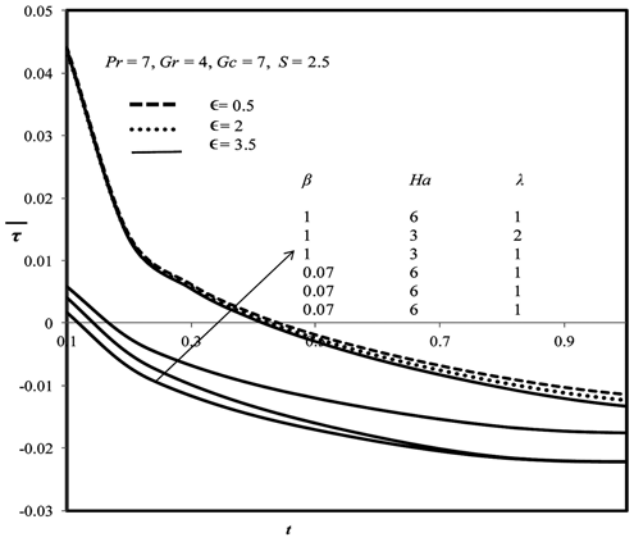

Fig. 7 – Average skin friction coefficient.

high friction force. The flow along the direction of Lorentz force with the gradually increased values of *Ha* deteriorates the viscous drag on account of high flow speed.

Local and mean heat transfer rate have been illustrated in Fig. 8 and 9. Rise in the values of constructive variable thermal conductivity parameter stimulates the heat transfer. In contrast to this, the destructive variable thermal conductivity parameter worsens the heat transport. As the flow is assisted by EMHD Lorentz force while increasing modified Hartmann number, the local and average Nusselt number values are improved eventually. Similarly, the exalted values of λ, β enhances the heat transfer between the molecules.

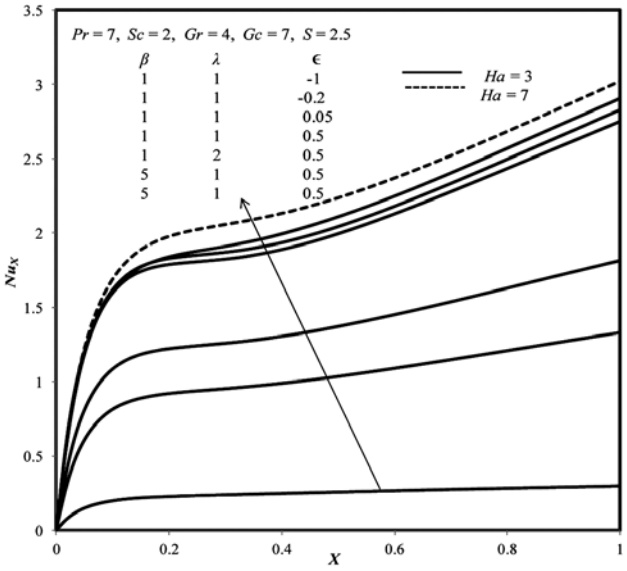

Fig. 8 – Local heat transfer rate.

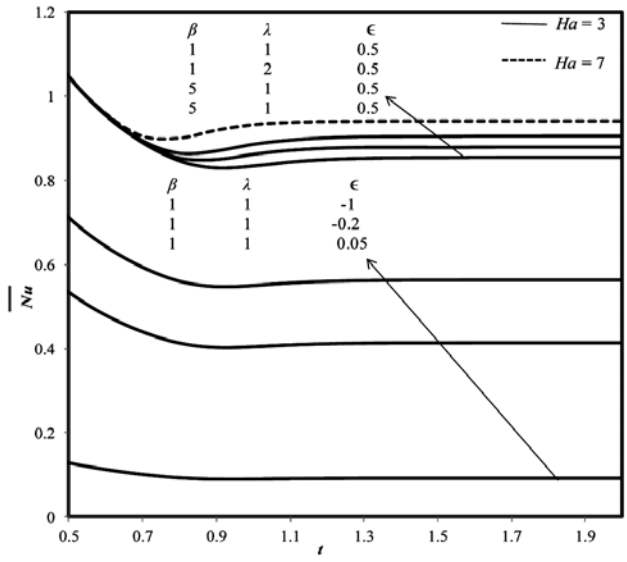

Fig. 9 – Mean heat transfer rate.

Figures 10 and 11 explicate the variations in Sherwood number. The high viscosity exerts an influence on the concentration gradient. This unveils the fact that the mass transfer rate escalated for higher values of Schmidt number. The magnetic field strength and electrical conductivity by virtue of the increase in modified Hartmann number improves the Sherwood number. On account of the stronger thermal conductivity, the lower mass transfer rate between the layers of the fluid is observed for improved values of variable thermal conductivity parameter.

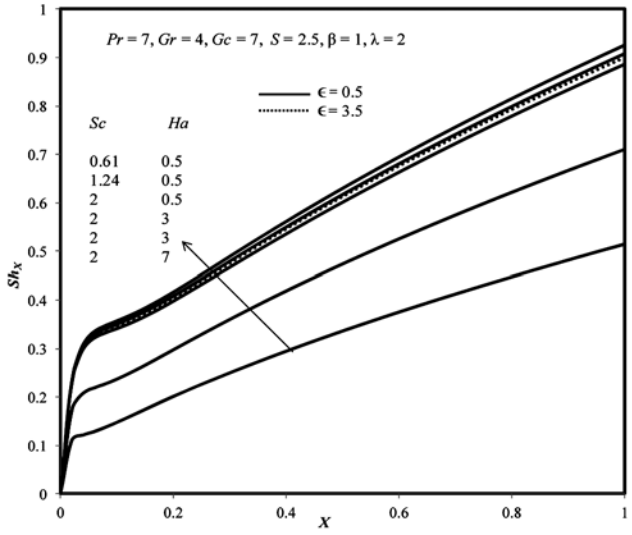

Fig. 10 – Local Sherwood number.

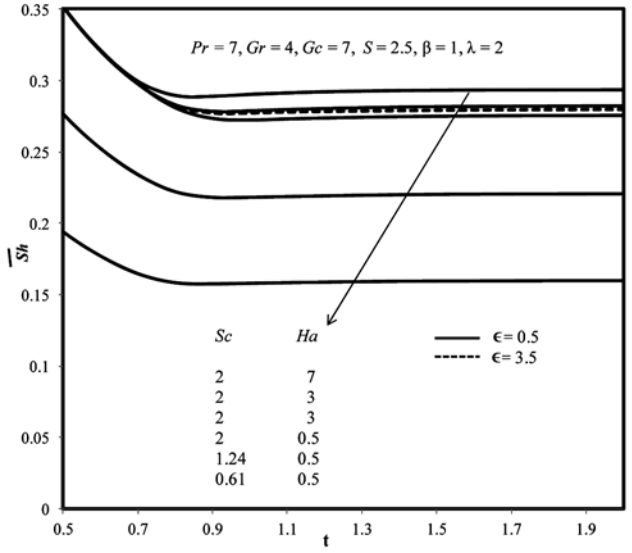

Fig. 11 – Mean Sherwood number.

5 Conclusions

Thermal conductivity is an indispensable transport property not only in the study of heat transfer, but it also has a control on the other flow properties. This detailed exploration prioritizes the impact of temperature dependent thermal conductivity on Casson fluid flow past a riga-plate. The recapitulations of distinctive results are rendered.

(i) Temperature dependent thermal conductivity improves the growth of momentum and thermal boundary layers. However, it diminishes the species concentration,

(ii) Modified Hartmann number escalates the flow speed, mass diffusion and induces the temperature drop,

(iii) Wall shear stress is reduced for the uplifted values of ϵ and *Ha,* but λ, β substantially raise τ_X,

(iv) Rate of heat transfer is lowered on the plate surface along the main stream velocity with constructive variable thermal conductivity. It shows an opposite effect for the destructive case and

(v) Uplifting modified Hartmann number enhances the Sherwood number and the trend is reversed for variable thermal conductivity parameter.

Acknowledgement

One of the authors, K Deepa immensely expresses the gratitude to Anna University, Chennai for supporting this research work through "Anna Centenary Research Fellowship".

References

1 Annaratone D, *Eng Heat Trans*, Springer, 2010.
2 Chaim T C, *Int Commun Heat Mass*, 23 (1996) 239.
3 Uddin Z & Kumar M, *Math Phys Comput Model*, 13 (2009) 15.
4 Mahanti N C & Gaur P, *J Appl Fluid Mech*, 2 (2009) 23.
5 Loganathan P, Ganesan P & Iranian D, *Int J Eng Sci Technol*, 2 (2010) 6257.
6 Iranian D, Loganathan P & Ganesan P, *Int J Comput Appl*, 121 (2015) 0975.
7 Hazarika S & Hazarika G C, *Int J Eng Sci*, 4 (2015) 20.
8 Thakur P M & Hazarika G C, *Int J Comput Appl*, 110 (2015) 0975.
9 Srinivasacharya D, Mallikarjuna B & Bhuvanavijaya R, *Alexandria Eng J*, 55 (2016) 1243.
10 Hayat T, Khan M I, Waqas M & Alsaedi A, *Results Phys*, 7 (2017) 446.
11 Dubovikova N, Karcher C & Kolesnikov C, *Proc Appl Math Mech*, 14 (2014) 721.
12 Weier T, Gerbeth G, Mutschke G, Lielausis O & Lammers G, *Flow Turbul Combust*, 71 (2003) 5.
13 Pantokratoras A, *Math Probl Eng*, 2008.
14 Pantokratoras A & Magyari E, *J Eng Math*, 64 (2009) 303.
15 Magyari E & Pantokratoras A, *Commun Nonlinear Sci*, 16 (2011) 3158.
16 Kumar K G, Haq R, Rudraswamy N G & Gireesha B J, *Results Phys*, 7 (2017) 3465.
17 Shah S, Hussain S & Sagheer M, *Results Phys*, 9 (2018) 303.
18 Afridi M I, Qasim M & Hussanan A, *Entropy,* 20 (2018) 615.
19 Cross M M, *J Coll Sci*, 20 (1965) 417.
20 Chhabra R P & Richardson J F, Non-Newtonian flow in the process industries; fundamentals and engineering applications, Butterworth-Heinemann publishing, 1999.
21 Srinivasa S, Kumar C K & Reddy A S, *Nonlinear Anal-Model*, 23 (2018) 213.
22 Zaib A, Bhattacharyya K, Uddin M S & Shafie S, *Model Simulat Eng*, 2016 (2016).

23 Animasaun I L, *J Heat Mass Trans Res*, 2 (2015) 63.
24 Animasaun I L, *J Niger Math Soc*, 34 (2015) 11.
25 Animasaun I L, Adebile E A & Fagbade A I, *J Niger Math Soc*, 35 (2016) 1.
26 Radha G, Bhaskar R N & Gangadhar K, *Int J Mech Solids*, 12 (2017) 235.
27 Mustafa M, Hayat T, Pop I & Aziz A, *Heat Trans Asian Res*, 40 (2011).
28 Rao M E, *IOP Conf Ser: J Phys*, 2018, doi: 10.1088/1742-6596/1000/1/012158.
29 Shehzad S A, Hayat T, Qasim M & Asghar S, *Brazil J Chem Eng*, 30(2013) 187.
30 Carnahan B, Luther H A & Wilkes J O, *Appl Numer Meth*, John Wiley and Sons, New York, 1969.
31 Smith G D, *Numerical solution of partial differential equations: finite difference methods*, Oxford University press, New York, 1985.
32 D'acunto, B, *Computational methods for PDE in mechanics*, world scientific publishing, Singapore, 2004.
33 Gebhart B & Pera L, *Int J Heat Mass Trans*, 14 (1971) 2025.